ACS Synthetic Biology
Cite This: ACS Synth. Biol. 2018, 7, 933−944
Research Article
pubs.acs.org/synthbio

An Automated Induction Microfluidics System for Synthetic Biology

Mathieu C. Husser,[†,‡] Philippe Q. N. Vo,[§] Hugo Sinha,[‡,§] Fatemeh Ahmadi,[‡,§] and Steve C. C. Shih*[,†,‡,§,∥]

[†]Department of Biology, Concordia University, Montréal, Québec H4B 1R6, Canada
[‡]Centre for Applied Synthetic Biology, Concordia University, Montréal, Québec H4B 1R6, Canada
[§]Department of Electrical and Computer Engineering, Concordia University, Montréal, Québec H3G 1M8, Canada

Supporting Information

ABSTRACT: The expression of a recombinant gene in a host organism through induction can be an extensively manual and labor-intensive procedure. Several methods have been developed to simplify the protocol, but none has fully replaced the traditional IPTG-based induction. To simplify this process, we describe the development of an autoinduction platform based on digital microfluidics. This system consists of a 600 nm LED and a light sensor to enable the real-time monitoring of the optical density (OD) samples coordinated with the semicontinuous mixing of a bacterial culture. A hand-held device was designed as a microbioreactor to culture cells and to measure the OD of the bacterial culture. In addition, it serves as a platform for the analysis of regulated protein expression in *E. coli* without the requirement of standardized well-plates or pipetting-based platforms. Here, we report for the first time, a system that offers great convenience without the user to physically monitor the culture or to manually add inducer at specific times. We characterized our system by looking at several parameters (electrode designs, gap height, and growth rates) required for an autoinducible system. As a first step, we carried out an automated induction optimization assay using a RFP reporter gene to identify conditions suitable for our system. Next, we used our system to identify active thermophilic β-glucosidase enzymes that may be suitable candidates for biomass hydrolysis. Overall, we believe that this platform may be useful for synthetic biology applications that require regulating and analyzing expression of heterologous genes for strain optimization.

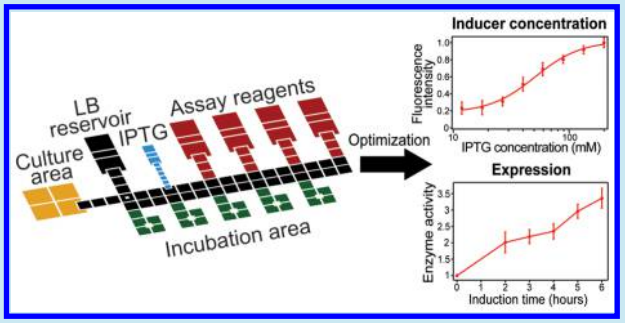

KEYWORDS: *automation, microfluidics, induction, synthetic biology, enzyme*

Using synthetic biology, several key biological functions can be engineered in living cells to yield valuable products such as therapeutic agents for diseases,[1−3] or biochemicals for green energy.[4,5] It follows a typical iterative engineering workflow of design−build−test−learn (DBTL) to simultaneously study a biological system while creating these useful technologies through rational design and assembly of DNA from varied sources. While the field of synthetic biology has advanced rapidly in recent years, certain technical challenges still exist like the development of strains due to difficulties in anticipating the combined effect of various DNA parts (*i.e.*, expression constructs) and assay conditions.[6,7] The engineering of viable strains relies on the characterization of genetic parts to attain optimal protein expression and productivity. As a result, numerous research groups have devoted much time into characterizing DNA parts by screening for their ability to confer improved phenotype. For example, many libraries of promoters (designed *via* mutagenesis) have been tested to regulate transcription rates and to improve overall protein expression.[8−11] Additionally, several inducible promoters have been designed in *E. coli* and in other types of bacteria that enable independent control over the expression of downstream genes.[12−14] Also, commercially available systems, like the pET expression system, are often used to control the expression of recombinant genes in *E. coli*. This system consists of a T7 promoter controlled by the lac operator that allows gene expression in the presence of an inducer[15,16] (*e.g.*, IPTG[17,18]). Using induction for the purpose of strain optimization usually involves growing a culture of cells with the desired exogenous constructs to an optimal optical density (OD), followed by the addition of an inducer. The cells are harvested after growth in the presence of the inducer and tested for the desired output, usually the expression of a protein of choice. In addition to the high costs of inducers, this is a manual and labor-intensive process, requiring frequent optimization of expression conditions, such as inducer concentrations and growth conditions, to achieve optimal levels of protein expression. Hence, the need for a more simplified and automated protocol would (1) eliminate the need to constantly monitor cell growth, (2) actively induce expression of the target gene at the appropriate time to obtain a desired level of expression, and (3) allow faster screening of parameters affecting recombinant protein expression to rapidly inform iterative strain optimization efforts.

Received: January 16, 2018
Published: March 8, 2018

DOI: 10.1021/acssynbio.8b00025
ACS Synth. Biol. 2018, 7, 933−944

A common practice to automate the expression of genes is to use an auto- or self-inducing system.[19−24] Autoinducible systems allow the culture to increase in density before induction of recombinant proteins since these systems are regulated by endogenous or induced metabolic changes during the growth. As opposed to IPTG-based manual induction methods, the autoinducing systems do not require monitoring of culture density and reduce the chances of contamination. Although improving upon the induction protocol, the auto-induction protocol removes the capability of control—*i.e.*, not knowing the cell density and the relative amounts of nutrient sources to induce protein expression. The inability to control these factors using autoinduction often leads to higher levels of target protein per volume of culture than standard approaches, which could cause a high metabolic burden and inhibit cell metabolism and growth and therefore critical to the outcome of protein expression.[25] Furthermore, the autoinducing system does not optimize or provide analysis of protein expression. Therefore, a technology that allows the flexibility of time and quantity of induction while simultaneously providing automation to monitor cell density and screening/analysis of different parameters that affect recombinant protein expression, may be a suitable alternative for controlling and improving protein yields.

Recently, a technology called microfluidics has been developed to miniaturize chemical and biological processes onto hand-held devices. Microfluidics have numerous advantages: reduction in volumes (1000× compared to bench techniques), high-throughput processing, and potential to automate fluidic processes. It has been applied to a host of applications such as cell-based monitoring, point-of-care diagnostics, and synthetic biology.[26−30] Traditionally, these devices have streams of μL-fluid flowing inside a micron-sized channel. An alternative to microchannels is digital microfluidics (DMF),[31−33] that uses an array of electrodes fabricated on a chip such that nL (or pL-range) volume droplets can be manipulated on the device. The versatility of DMF enables control over the droplets—dispensing, splitting, merging, and moving droplet operations—and therefore is a natural fit for automating fluid handling operations related to synthetic biology since it has the capability of integrating and automating the DBTL cycle into a coherent whole.[34−36]

Here, we have designed the first automated induction microfluidics system (AIMS) for synthetic biology to provide a platform that will optimize and analyze parameters affecting expression of proteins. Our system encompasses three components: (1) a DMF platform to culture and to induce biological cells and to analyze protein expression, (2) an automation system to drive droplet movement on the DMF device, and (3) an absorbance reader to monitor the optical density (OD) of the cells. This new technique is automated such that cell culture, OD monitoring and measurement, induction, and testing protein expression are all conducted on chip without manual intervention. This system also presents additional advantages for gene expression protocols as it minimizes chances for cross-contamination, presents greater control over experimental conditions, allows additional cultures to be induced simultaneously, and reduces significant costs for inducers (like IPTG) by minimizing the volumes required for induction. Although AIMS is built for IPTG-based induction to facilitate OD monitoring, it can be used with other inducible systems[37] or autoinducible expression system[22] (*e.g.*, automating all fluidic operations to control conditions for protein expression without the need of an inducer). Below, we describe a proof-of-principle implementation of an automated workflow to test a variety of induction conditions to determine the levels of protein expression of a red-fluorescent protein (RFP) gene. We also demonstrate the utility and versatility of the AIMS by testing the activity of key β-glucosidase (BGL) genes from *Thermomicrobium roseum*, *Thermobaculum terrenum*, and *Rhodothermus marinus*[38] that may be useful in biomass hydrolysis for biofuel production.

MATERIALS AND METHODS

Reagents and Materials. All general-use reagents were purchased from Sigma, unless specified otherwise. *E. coli* DH5α and BL21(DE3) strains and original pET16b vectors were generously donated from Dr. Vincent Martin. Strain and plasmids used for this study are shown in Table S1 (Genbank sequence files provided in Supporting Information; plasmids also made available from Addgene and ACS Synthetic Biology registry). Miniprep kits (cat no. BS413) and gel extraction kits (cat no. BS354) were purchased from BioBasic (Amherst, NY). β-glucosidase substrate 4-methylumbelliferyl β-D-glucopyranoside (MUG) was purchased from Carbosynth (cat no. EM05983, San Diego, CA).

Microfluidics device fabrication reagents and supplies included chromium coated with S1811 photoresist on glass slides from Telic (Valencia, CA), indium tin oxide (ITO)-coated glass slides, R_S = 15−25 Ω (cat no. CG-61IN-S207, Delta Technologies, Loveland CO), FluoroPel PFC1601 V from Cytonix LLC (Beltsville, MD), MF-321 positive photoresist developer from Rohm and Haas (Marlborough, MA), CR-4 chromium etchant from OM Group (Cleveland, OH), and AZ-300T photoresist stripper from AZ Electronic Materials (Somerville, NJ). Transparency masks for device fabrication were printed from CADArt (Bandon, OR) and polylactic acid (PLA) material for 3D printing were purchased from 3Dshop (Mississauga, ON, Canada).

Plasmid Preparation and Transformation. The gene sequence for the reporter red fluorescence protein (RFP) was obtained from the iGEM registry (BBa_E1010) and the β-glucosidase genes (BGL) from *Thermomicrobium roseum* (BGL1, GenBank accession number YP_002522957.1), *Thermobaculum terrenum* (BGL2, GenBank accession number WP_041425608.1), and *Rhodothermus marinus DSM4252* (BGL3, GenBank accession number WP_012844561.1). BGL1 was synthesized by IDT (Coralville, IA) as a linear DNA fragment, and BGL2 and BGL3 were synthesized by Gen9 (now Ginkgo Bioworks). These genes were used for amplification by PCR (see Table S2 for primer sequences). Individual PCR reactions consisted of 10 μL 5X Phusion buffer, 1 μL dimethyl sulfoxide (DMSO), 20 ng template DNA, individual dNTPs and primers to a final concentration of 200 μM and 0.5 μM each, 0.5 μL Phusion polymerase and distilled water up to 50 μL. The following PCR thermocycling conditions were used: initial denaturation at 98 °C for 30 s followed by 35 cycles of denaturation at 98 °C for 10 s, annealing at 55 °C for 30 s and extension at 72 °C for 30 s/kb, and a final extension step at 72 °C for 10 min. PCR products were loaded into a 0.8% agarose gel in TAE buffer and resolved at 130 V for 30 min. The corresponding bands from a gel (Figure S2) were extracted using a gel extraction kit. The recovered DNA was digested using XbaI and *Bam*HI restriction enzymes (Thermo, Waltham, MA) for 4 h at 37 °C and ligated into a pET16b expression vector that contains a T7 promoter

DOI: 10.1021/acssynbio.8b00025
ACS Synth. Biol. 2018, 7, 933−944

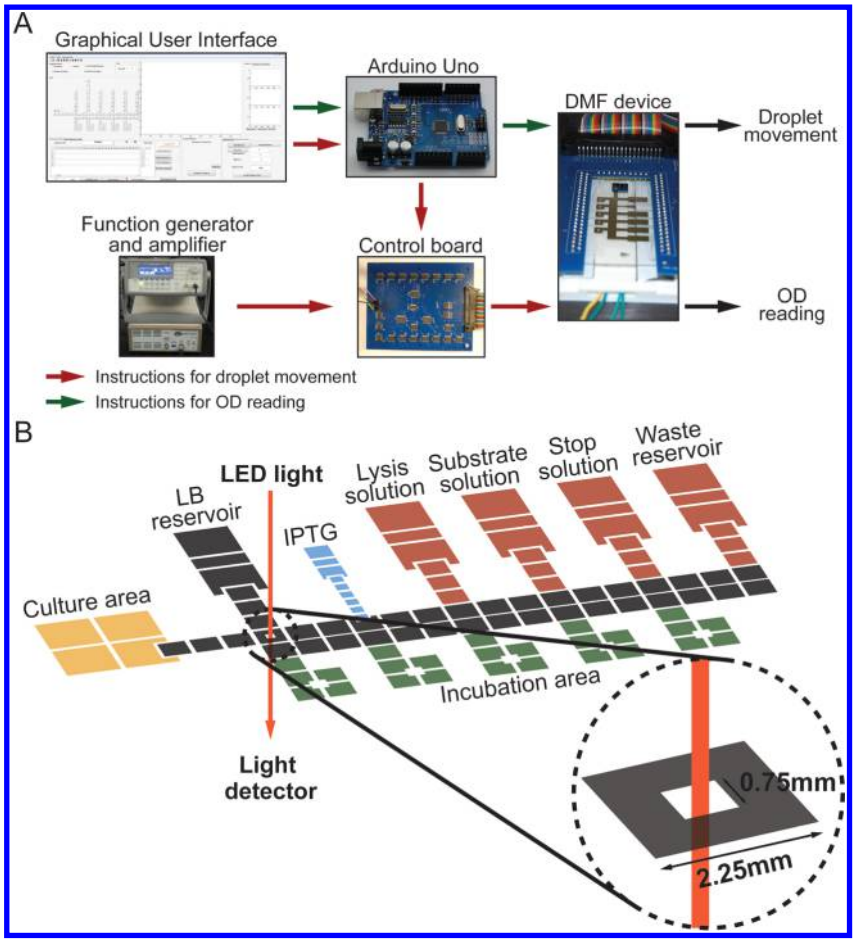

Figure 1. Automated Induction Microfluidics System (AIMS). (A) The schematic illustrates the relationships between the function generator and amplifier, the control board bearing the solid state switches for high voltage, the Arduino Uno, the pogo pin board and the DMF device. Low voltage signals (5 V DC) are delivered to the Arduino to activate the switches on the control board to deliver high voltage (~100 V_{RMS}) to the DMF device *via* pogo pins. To automate cell culture, induction, and analysis of protein expression, user programs a droplet movement sequence by clicking on the graphical user interface to initiate droplet movement. (B) Schematic of the device. A cell culture area bearing four square electrodes (4.5 × 4.5 mm each) are used to semicontinuously mix the mother culture droplet. To monitor OD, the mother droplet is extended to the absorbance reading electrode (bottom, expanded view). If the OD reading surpasses the threshold, a droplet of IPTG is dispensed and mixed with a daughter droplet. Next, this will start one of two programs: concentration or time-course which will initiate droplet movement sequences and start incubation in the assay regions.

and lacI coding sequence using T4 ligase (Thermo, Waltham, MA) for 1 h at room temperature (see Figure S3 for plasmid map). For transformation, 100 μL of thawed competent cells were mixed with 100 ng of the ligation product and placed on ice. This mixture was heat-shocked at 42 °C for 45 s after which cells were placed on ice for 1 min for recovery. 900 μL of LB media were added to each transformation mixture and the cells were incubated at 37 °C for 1 h. 200 μL of the final mixture were plated onto selective LB agar plates containing 100 μg/mL ampicillin (Amp) and incubated at 37 °C overnight. Single colonies were picked the following day and inoculated into 5 mL of LB Amp overnight. Plasmids containing RFP and BGL genes were extracted from *E. coli* using a miniprep kit and were digested with XbaI and *Bam*HI and verified on a gel to ensure proper insertion of the genes.

Conventional Benchtop Culture, Induction, and Expression. Chemically competent *E. coli* BL21(DE3) cells were transformed with the expression vector containing the cloned genes for induction. Cultures from single colonies were grown in 5 mL of LB media containing 100 μg/mL Amp shaking at 200 rpm with constant 37 °C temperature overnight. These were diluted to a starter culture of OD 0.1 and grown under the same conditions until they reached an OD of 0.4. An optical density (with replicates) at 600 nm was measured periodically in microcentrifuge tubes on a Varian Cary 50 Bio UV−vis spectrophotometer (Agilent Technologies, Santa Clara, CA). To initiate gene expression, the cultures were induced by adding 1 mM IPTG at OD 0.4 and were incubated under the same conditions for 4 h. Induced cultures were then collected in conical centrifuge tubes and stored at −20 °C for later use.

To obtain a macroscale growth curve, a 150 mL culture was started by diluting an overnight culture carrying an empty pET16b vector to OD 0.1 in selective media. The macroscale culture was incubated at 37 °C with 200 rpm shaking. The flask was taken out every 30 min to measure the optical density of triplicate 1 mL samples. OD was measured at 600 nm on the Varian Cary 50 spectrophotometer. The experiment was carried out until OD reached a plateau, and a growth curve for the macroscale culture was plotted. Since we are culturing cells in Pluronics F-68 on microfluidics, we tested the effects of Pluronics F-68 on bacteria growth and discovered no detrimental effects on their growth (Figure S4).

DOI: 10.1021/acssynbio.8b00025
ACS Synth. Biol. 2018, 7, 933−944

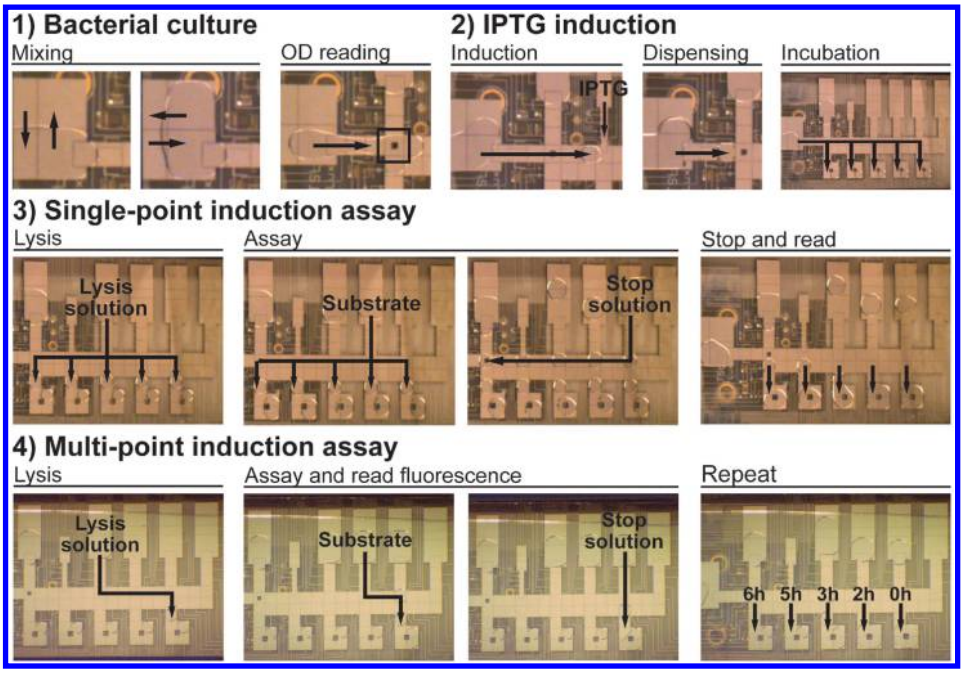

Figure 2. Sequence of droplet operation using AIMS. Images from a movie of the device in action. In (1) the mother drop was mixed by the AIMS interchanging vertical and horizontal directions. The mother drop was extended and actuated to the absorbance window to measure the OD of the culture. (2) A droplet of IPTG is dispensed and mixed with the mother culture droplet. Five daughter droplets are then dispensed and incubated in the five assay areas. (3) The BGL assay consisted of the successive mixing of the induced culture with a lysis solution, incubation with the MUG substrate, followed by the addition of a stop solution. See Video S1 (Supporting Information) showing the droplet movement steps for a single-point induction assay.

For inducer concentration optimization macroscale experiments, starter cultures transformed with a RFP plasmid were prepared at OD 0.1 from overnight inoculations. The cultures were grown at 37 °C with shaking and were induced upon reaching OD 0.4. 45 mL of the culture was induced at 200 μM and diluted with fresh media to generate the following IPTG concentrations: 200, 133.3, 88.9, 59.3, 40, 26.7, 17.8, and 11.9 μM. These subcultures were prepared in triplicates along with a noninduced control and were induced at 37 °C and shaken for 4 h. After induction, 200 μL of each culture were loaded onto a 96-well plate and fluorescence at 612 nm was measured with 582 nm excitation on a TECAN Infinite M200 plate reader (Mannedorf, Switzerland) with the settings: gain of 75, 25 flashes and 20 μs integration time. The fluorescence intensity with increasing IPTG concentration was plotted on a logarithmic scale to generate a dose−response curve.

Microfluidic Device Fabrication. Devices were designed using AutoCAD 2016 (Autodesk, San Rafael, CA) and fabricated in the Concordia Silicon Microfabrication Lab (ConSIM). The fabrication procedure followed a previous protocol[39] using high resolution 25,400 dpi transparency masks printed by CAD/Art sevices. Briefly, glass substrates precoated with S1811 photoresist (Telic, Valencia, CA) were exposed to UV for 8 s on a Quintel Q-4000 mask aligner (Neutronix Quintel, Morgan Hill, CA) to imprint the transparency masks design. These were developed in MF-321 for 2 min with shaking and rinsing with DI water. Developed slides were then baked at 115 °C for 1 min before etching in CR-4 chromium etchant until the pattern was clearly visible. The remaining photoresist was then removed in AZ-300T stripper for 2 min. After rinsing with DI water and drying, a silane solution comprising deionized water, 2-propanol and (trimethoxysilyl)-propyl methacrylate (50:50:1) was added to the devices in a pyrex dish for 15 min. Devices were primed for dielectric coating with Parylene-C (7.2 μm) in a SCS Labcoter 2 PDS 2010 (Specialty Coating Systems, Indianapolis, IN), and coated with Fluoropel PFC1601 V (Cytonix, Beltsville, MD) in a Laurell spin coater (North Wales, PA) set to 1500 rpm for 30 s with 500 rpm/s acceleration followed by 10 min baking at 180 °C.

Automated Induction Microfluidics System (AIMS). As depicted in Figure 1A, the AIMS was combined with other electrical hardware components with in-house software to automate cell culture, induction, and analysis. The AIMS was comprised of a 3D printed top cover with a 600 nm LED (Digikey, Cat no. 1497−1021-ND, Winnipeg, MB) and a bottom holder (see Figure S1 for design and SI for top and bottom holder fabrication) containing a luminosity sensor (TSL2561, Adafruit, New York, NY). To measure optical density, devices are placed in a slot in the bottom holder that is approximately 8 mm below the LED and 4 mm above the lux sensor. Alignment marks were designed on the device and on the bottom holder to align the absorbance window on the device with the lux sensor to minimize fluctuations in the lux measurements. The lux sensor was programmed (code is made available on GitHub, www.github.com/shihmicrolab/AIMS) and managed using an Arduino Uno controller connected to the graphical user interface to display the measured luminosity values.

Droplet motion on our devices was managed using an automated control system (hardware and software available on GitHub; Table S3 for BOM list).[40] It consists of a custom MATLAB (Natlick, MA) program interfaced to an Arduino Uno that controls the states of a network of high-voltage relays (AQW216 Panasonic, Digikey, Winnipeg, MB). The control board is connected to a function generator (33201A Agilent,

DOI: 10.1021/acssynbio.8b00025
ACS Synth. Biol. 2018, 7, 933−944

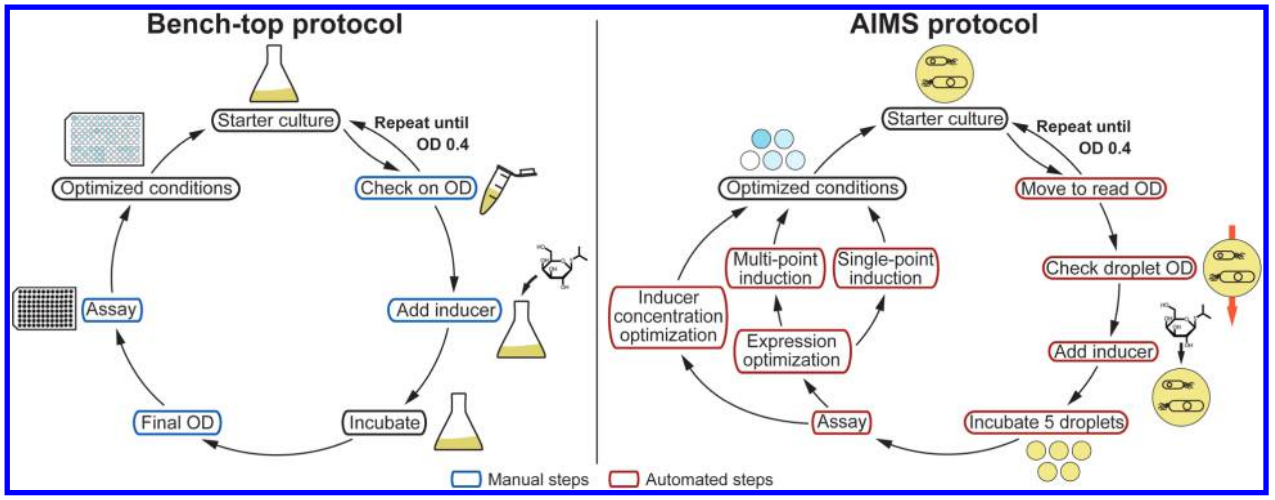

Figure 3. Comparison of the conventional and microfluidic induction protocol. The conventional protocol uses large volumes (~mL) to start the cell culture and frequently requires manual monitoring of the OD (μL volumes). Once the culture reaches the threshold OD, the user pipettes an aliquot of an inducer (*e.g.*, IPTG) into the culture and continues culturing until ready for a biological assay. Typically, the user requires another liquid handling platform for the biological assay (*e.g.*, well-plate). The AIMS protocol only requires initial pipetting steps (reagents, cells in media, inducer) while all other induction and assay steps are automated. The "Inducer concentration" program was used to optimize IPTG concentrations, and the "Expression optimization" program was used to screen different enzymes (Single-point induction) and expression conditions of the highest active enzyme (Multipoint induction). See Figure 2 for the droplet movement protocol using the AIMS.

Allied Electronics, Ottawa, ON) and a high-voltage amplifier (PZD-700A, Trek Inc., Lockport, NY) that delivers 130−270 V_{RMS} sinusoidal signals to the mated pogo-pin board. Specifically, the inputs of the relays are connected to the function generator/amplifier combination and the outputs are mated to the pogopin board. Controlling the logic of the individual switches is done through an I^2C communication protocol using an I/O expander (Maxim 7300, Digikey, Winnipeg, MB). In practice, the user inserts the device into the OD reader, loads the reagents onto the device, and then inputs a series of desired droplet movement steps such that induction (and cell culture and analysis) will be performed automatically by the AIMS. A list of components used to manufacture a microfluidics control system is included in the Supporting Information (Table S3).

Microfluidic Automated Culture, Induction, Expression. The above protocols for the conventional benchtop experiments were adapted to the volumes used on the microfluidic device and supplemented with 0.05% Pluronics F-68. Pluronics additives are necessary as they prevent any proteins or cell adsorption on the DMF device.[41−43] Prior to the experiment, the device (Figure 1B) was inserted between the OD reader of the AIMS setup and the pogo pin interface. A droplet containing media with cells was loaded onto the mother culture area and the bottom plate was mated with an ITO top plate for grounding to complete the device configuration. During the experiment, this setup was placed in an incubator to maintain the system temperature at 37 °C, with an open water container to provide humidity and to prevent droplet evaporation on the device.

To generate a growth curve, the mother culture was initialized by diluting an overnight culture with fresh media containing 0.05% Pluronic F-68 to a low OD (~0.1). 14 μL of this culture were loaded onto the culturing area of the DMF device and was semicontinuously mixed at a frequency of one actuation every 45 s (with 700 ms of actuation time) to ensure uniform cell density in the mother culture (Figure 2, Mixing). Illuminance measurements (lux) were carried out from the absorbance window on the device using the luminosity sensor. A blank (*i.e.*, a droplet of LB media and no cells) value was acquired before every sample reading to calculate the OD, using the equation:

$$A = \log\left(\frac{I_0}{I}\right)/0.028$$

where A is the measured absorbance in OD, I_0 is the blank light intensity value, and I is the light intensity reading from the sample. The OD value is divided by 0.028 to correct for the path length of readings across the 280 μm of height gap.

During a period of cell growth, induction is then required to initiate protein expression. The induction procedure starts with actuating the mother droplet containing the bacteria to the absorbance window to measure the OD (Figure 2, OD reading). If the calculated OD is below our threshold OD of 0.4, the mother culture would go back to the mixing area and continue mixing for 10 min until the next OD reading. However, if the OD reaches the threshold, the control system would trigger an induction program to start by dispensing a droplet of IPTG to mix with the culture. This will initiate one of two programs: inducer concentration or expression optimization program.

In the inducer concentration optimization program, three unit droplets of 1.42 μL containing transformed RFP-cells were dispensed from the culture region and mixed with 0.3 μL of 3.24 mM IPTG. This droplet was actuated to an empty reservoir and one daughter droplet was split from this reservoir and actuated to the incubation region. Another unit droplet from the mother culture was then mixed into the reservoir and split again to generate 2:1 serial dilutions of IPTG. After each split, the droplets were actuated to their respective assay spot. To assess the impact of IPTG concentration on gene expression, the RFP expression was evaluated after 4 h by placing our device on top of a well-plate cover and then inserted into in a CLARIOStar plate reader (BGM labtech, Ortenberg, Germany) to measure fluorescence emission at 612 nm with excitation at 582 nm using a well scanning program

DOI: 10.1021/acssynbio.8b00025
ACS Synth. Biol. 2018, 7, 933−944

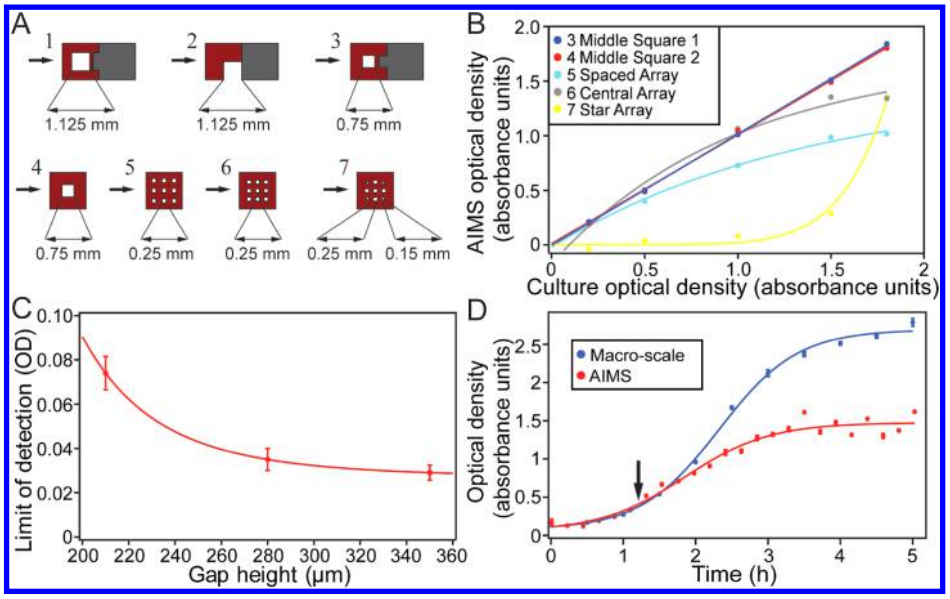

Figure 4. Characterization of the AIMS. (A) Schematic of the different absorbance windows tested in this study. (B) Calibration curve of bacterial cultures of different OD were measured in a spectrophotometer. The same samples were verified with our AIMS system. (C) A curve showing the limit of detection for a given interspacer height (between top and bottom plate). The limit of detection was calculated by measuring the OD using the AIMS of a blank sample (*i.e.*, media with no cells) and adding three times the standard deviation. (D) Representative growth curves of bacteria on the benchtop or using the AIMS. Benchtop measurements were conducted using a well-plate reader and grown in flasks while microscale measurements were conducted on the AIMS. The arrow indicates the point of induction (OD = 0.4). For (B–D), error bars represent ±1 standard deviation across triplicates.

with scan matrix = 30 × 30, scan width = 6 mm, a focal height = 7.2 mm, and with a gain = 2905.

In the expression optimization program, two assays (single-point and multipoint) were conducted to show the utility of our system and to identify highly active BGL enzymes. In single-point induction, a 2 μL droplet of 11 mM IPTG was mixed with a single culture droplet, which was then returned to the culture mixing area to mix and induce the entire culture (Figure 2, Induction). Five induced daughter droplets were dispensed and actuated to their respective incubation spots (Figure 2, Incubation). After 4 h of induction, each of the droplets on the spot was mixed with a 1.42 μL 1× lysis solution droplet to break open the cells to analyze the BGL enzymes (Figure 2, Lysis). After 10 min of lysis at room temperature, a 1.42 μL droplet containing 150 mM sodium-citrate and 6 mM MUG was added to each assay area and were incubated for different durations (0, 15, 30, 45, and 60 min). The reaction was stopped by the addition of a 1.42 μL droplet of 0.4 M glycine–NaOH (Figure 2, Stop and Read Fluorescence). To assess the BGL activity, the device was placed on a well-plate cover and into a well-plate reader to measure the fluorescence intensity at 449 nm upon 368 nm excitation, with the same settings as in the inducer concentration program except for a focal height of 4.0 mm and gain of 664. The fluorescence intensity of each droplet was taken for analysis.

In the multipoint induction assay, a culture of low OD (~0.1) was grown and induced with the same volume and concentration as in the single-point program. Upon induction, five subcultures were lysed and assayed after 0, 2, 3, 5, and 6 h of induction (Figure 2, Multipoint induction assay). Lysis was carried out for 10 min and each droplet was incubated with MUG for 30 min before quenching and fluorescence reading. The same settings were used for fluorescence measurement as in the single-point induction assay.

RESULTS AND DISCUSSION

Characterization of the AIMS. A wide range of synthetic biology applications such as strain optimization require the use of induction. One example is to study biological parts or tools affecting recombinant protein expression in *E. coli* or yeast to improve protein yields or understand patterns of gene expression.[11,44−47] Typically, induction follows a manual procedure with constant monitoring of cell density and manual addition of the inducer at a specific time point. Here, we present the first automated induction system using digital microfluidics that is capable of culture, induction, and protein analysis without these manual steps (Figure 3). We call this system AIMS, after its function "automated induction microfluidics system".

The primary function of the AIMS is to automate induction, which requires initial cell culturing. As shown in Figure 1B, the device was designed such that cell culture takes place in a 20 μL droplet containing media and cells (with a starting OD of 0.1), which we term "mother culture". In initial experiments, the mother culture was continuously mixed to ensure uniform distribution of gases and nutrients and especially the cells themselves.[48,49] However, we observed biofouling after 2 h of culturing which was not enough to reach the OD for induction. It has been reported elsewhere[50−52] that droplets can be semicontinuously mixed which can reduce biofouling,[41] with droplet contents being mixed at rates up to 10–50× faster than diffusion alone using an array-based format of electrode.[50] As shown in Figure 2, the mixing step comprised of sequence of four movements that moved the mother culture in a horizontal and vertical directions. There are possibilities of moving the droplet in a more complex rearrangement (*e.g.*, figure-eight)[50] or resonating the droplet.[53] However, these either require more actuations or allowing the droplet to rest which may lead to faster biofouling on the device.[41] We initially tried faster actuation times <700 ms but the droplet would not move to the

DOI: 10.1021/acssynbio.8b00025
ACS Synth. Biol. 2018, 7, 933–944

activated electrode or slower actuation times but the droplet would biofoul the surface preventing further droplet movement. A balance is struck at 0.7 s (and every 45 s mixing frequency) when droplets would move while preventing any biofouling. Furthermore, the simple horizontal and vertical movement was adequate for induction and analysis since it provided a homogeneous distribution of the cells in the droplet.

Next, to facilitate absorbance measurements we tested a variety of different shaped electrodes for cell density analysis. As shown in Figure 4A, we tested seven different transparent windows for measuring OD. There are two criteria that we used to determine the optimal electrode: (1) droplets move reliably onto the electrode, and (2) the range of OD measurements that can be accurately measured (*i.e.*, resolution). To test droplet movement, a droplet from the mother culture was dispensed and actuated to the transparent electrode. Most of the evaluated electrodes (2−7) did not hinder droplet movement as the droplets reliably moved over the window. However, for electrode 1 (*i.e.*, a window consisting of 1.125 mm), droplets were either sluggish in their movement or did not move over the window. This electrode was designed with a transparent region that is 1/2 of the area of the square electrode, which is not a favorable since electrodynamic forces that are required to move the droplet are weaker when the electrode area is reduced.[54,55] Overall, most reliable movement on top of the absorbance electrode was observed by extending the mother culture onto the electrode rather than dispensing (Figure 2, OD reading). Next, we tested the range of OD measurements that can be observed with windows 2−7. We created dilutions of a bacterial cultures with different ODs (confirmed by our Varian Cary 50 Bio UV−vis spectrophotometer) and measured their OD with the AIMS. As shown in Figure 4B, we plotted the results of the verification for multiple OD samples. We observe the star-array window (electrode 7) did not give the expected linear range of values, which was also observed with the central (electrode 6) and the spaced (electrode 5) array. This is most likely due to the central transparent window being too small for reproducible measurements.[51] However, using a middle square electrode (electrodes 3 and 4) showed favorable results in terms of linearity, resolution, and accuracy. Table 1 shows the summary of our results and while the strategy of using a middle electrode worked well in the current design, future possibilities include integrating optical fibers[56] or waveguides[57] to increase the sensitivity of our measurements.

Table 1. Comparison of Criteria for Different Transparent Electrodes Used for Absorbance Measurements

number	description of transparent window	droplet movement?	slope	r^2
1	Large middle square	NO	NA	NA
2	Corner square	YES	NA	NA
3	Small middle square 1	YES	1.016	0.999
4[a]	Small middle square 2	YES	0.998	0.999
5	Spaced array	YES	1.1[b]	0.997[b]
6	Central array	YES	0.7[b]	0.999[b]
7	Star array	YES	NA	NA

[a]The chosen absorbance window used for AIMS. [b]These values were obtained from the linear portion of the standard curves.

An advantage of using digital microfluidics for automated induction is that we can easily adjust the vertical path length for absorbance measurements. Ideally, the larger the path length, the more sensitive the measurements will be at low absorbance (due to Beer−Lambert law). Here, we tested three different gap heights and measured the limit of detection of the OD measurements using AIMS. Initially, we tried small spacer thicknesses <140 μm between top and bottom plates in the devices since it is range of gap heights typically used for biological assays on DMF devices.[36,39] However, at these lower gap heights, we could not achieve sensitive and reproducible OD measurements. This led us to try larger heights (210, 280, and 350 μm) to determine the limit of detection by measuring the OD for droplets containing only media. As expected, a gap height of 350 μm gave the lowest limit of detection, 0.029 OD units (Figure 4C). However, a commonly observed problem at these gap heights on our devices is the reliability of dispensing. In fact, droplet dispensing for the media with cells and the repetitive dispensing from a reservoir were nearly impossible. We also tried increasing the voltage to improve droplet movement and dispensing (as suggested by others[58,59]), but this frequently led to electrolysis (*i.e.*, dielectric breakdown) on the device. Therefore, a 280 μm spacer was used for the work reported here since it gave an appropriate limit of detection and was reproducible in terms of droplet dispensing and movement.

To ensure induction at proper times, we compared the growth rates of bacteria on the AIMS to those cultured by conventional means. As described in the Materials and Methods section, the culture conditions of both systems were similar. As shown in Figure 4D, the growth of bacteria had a similar trend in the exponential region of the curve but showed significant differences in doubling times with 36.80 ± 0.36 and 72.88 ± 2.30 min for conventional and AIMS cultures respectively (two-tailed paired *t* test; *P*-value = 0.018). We did observe differences in the stationary phase and speculate that the variations in this phase between the micro- and macroscale systems may be caused by a number of factors. The most likely factor is the mixing efficiency since we are semicontinuously mixing on the microfluidic device while continuously mixing in the macroscale. Differences in mixing can result in differences in dissolved gases and nutrients in the culture which can make the bacteria cells enter the stationary phase faster than expected. In addition, the shorter path lengths in the microscale compared to the macroscale (280 μm *vs* 1 cm) can also give rise to variances in the OD measurements. Although we observed differences in the stationary phase, induction occurs in the early exponential phase (~0.3−0.4 OD) which is similar in both platforms.

Inducer Concentration Optimization: Monitoring Gene Expression. A key advantage of the AIMS is the potential of analyzing protein expression after induction directly on the same device. To illustrate this point with the AIMS, we tested our system with an IPTG inducible expression vector carrying a red fluorescent protein (RFP) gene downstream of a T7 promoter. Bacterial cells were cultured until OD 0.4 and induced using different IPTG concentrations (generated on-chip) to evaluate the optimal concentration for induction (Figure 5A). As shown, the dose−response curve in both macroscale and microfluidics devices followed a sigmoidal profile (*i.e.*, Hill function) with highest protein production after 4 h at IPTG concentrations above 200 μM. At lower concentrations of IPTG (typically <30 μM), protein production was constant (*i.e.*, basal levels), which is expected at these concentrations. We do observe some differences in the shapes of the curves, specifically in their steepness. This is not a surprise given the significant differences between both systems

DOI: 10.1021/acssynbio.8b00025
ACS Synth. Biol. 2018, 7, 933−944

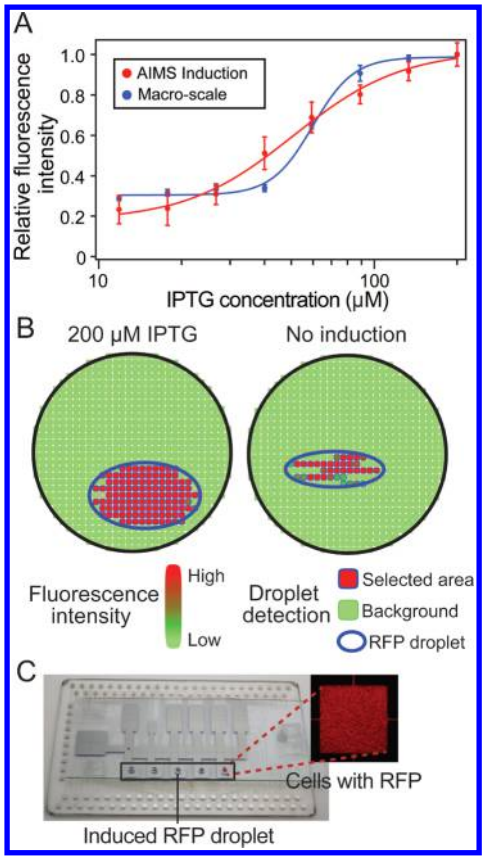

Figure 5. Inducer concentration optimization. (A) Comparison of the dose−response curves of IPTG using the AIMS and in macroscale cultures. Error bars represent ±1 standard deviation across triplicates. (B) RFP signal detected by fluorescent scan over an induced and noninduced droplet of culture. Fluorescence was measured with an excitation wavelength of 582 nm and an emission wavelength of 612 nm (refer to methods for specific well-plate settings). (C) Picture showing five regions on the device that contain droplets that were induced with IPTG. An expanded inset shows a droplet in the assay area with cells expressing RFP.

(in terms of volumes, E-field actuation, optical detectors, mixing efficiency of samples, *etc.*) However, this can be improved by integrating "sensitivity tuners"[60] or adding multiple protein-binding domains[61] or transcriptional cascade systems[62] into the cell that will adjust the effective binding cooperativity and improve cooperative binding of multiple transcription factors to the same promoter for transcriptionally regulated gene expression. Despite these differences, our system is capable of automating induction and monitoring gene expression, which can be extended to other types of induction assays (see Expression Optimization section).

Since fluorescence is used as a read-out for the protein production, we used an optical plate reader for analysis since our devices can be easily integrated with offline detectors.[51,63] Using these optical detectors, we can detect only the droplet area and therefore there is no risk of other fluorescent signals interfering with the desired signals. In addition, this readout is the last step of our process and therefore only required the transfer of the device into the plate reader—*i.e.*, no additional pipetting steps or fluid handling steps are needed. As shown in Figure 5B, the droplet can be selected by the well-plate software and can clearly distinguish between the droplet and its surrounding area and the difference between a low-fluorescence (no IPTG) and a highly fluorescent droplet (200 μM IPTG). This shows that our device is compatible with external detectors and can be used as an alternative for end-point fluorescence detection. In the future, we propose to integrate in-line fluorescent detectors[64] or variations of other types of assays which require induction and use absorbance of fluorescence as a readout, *e.g.*, genetic element screening[65,66] and/or tuning gene expression.[46,67]

As depicted in Figure 5C, the method was carried out in a 5-plex format, but in the future, we propose that it would be possible to expand the AIMS to even higher levels of multiplexing, particularly with the report of "hybrid" microfluidic techniques which can increase throughput and analysis of 1000s of samples.[39,68] In addition, the method reported here enables 10 000-fold reduction in bacterial culture volumes compared to bench-scale methods (15 μL in microscale *vs* 150 mL in batch scale) and at least 40-fold reduction in assay volumes (5 μL on the device compared to 200 μL in a 96-well plate). This system also enables an automated induction and gene expression analysis without intervention. We propose that the new methods described here may be particularly useful for applications involving precious and costly reagents and for induction assays that require multiple dilutions (see Table 2 for comparisons in costs, pipetting steps, and hands-on time).

Expression Optimization: Screening Active BGL Enzymes. Given the versatility of the AIMS, it is designed to analyze protein expression of more complex biological systems. There has been a surge of interest in discovering enzymes for breaking down large sugar polymers (consisting of hexose and pentose sugars) that can be fermented into biofuels as potential substitutes for gasoline, diesel, and jet fuel.[69−71] One group of enzymes, β-glucosidases (BGL) have attracted considerable attention in recent years due to their ability to hydrolyze cellulose to produce glucose. Typically, BGL activity is first measured using artificial substrates such as 4-methylumbelliferyl β-D-glucopyranoside (MUG). Hence, we used the AIMS to investigate the catalytic activity of three BGLs based on the artificial substrate MUG (see Figure 6A for chemical scheme). To start, three reagent reservoirs were dedicated to the dispensing of multiple reagents (substrate, lysis solution, and

Table 2. Comparisons in Cost, Time, and Manual Intervention for the Macro- and Microscale

	macroscale			AIMS		
level of multiplexing	costs[b]	pipetting steps	hands-on time (min)	costs[b]	pipetting steps	hands-on time (min)
5	$2.52/$8.02	32	35	$0.01/$4.51	18	18
100[a]	$18.83/$24.33	621	370	$0.24/$4.74	135	50
1000[a]	$188.28/$248.78	6021	930	$2.45/$47.45	1215	235

[a]Not performed in this study—estimated values (see Supporting Information). [b](left) Costs for reagents; (right) costs for reagents and consumables (*e.g.*, plates and devices).

DOI: 10.1021/acssynbio.8b00025
ACS Synth. Biol. 2018, 7, 933−944

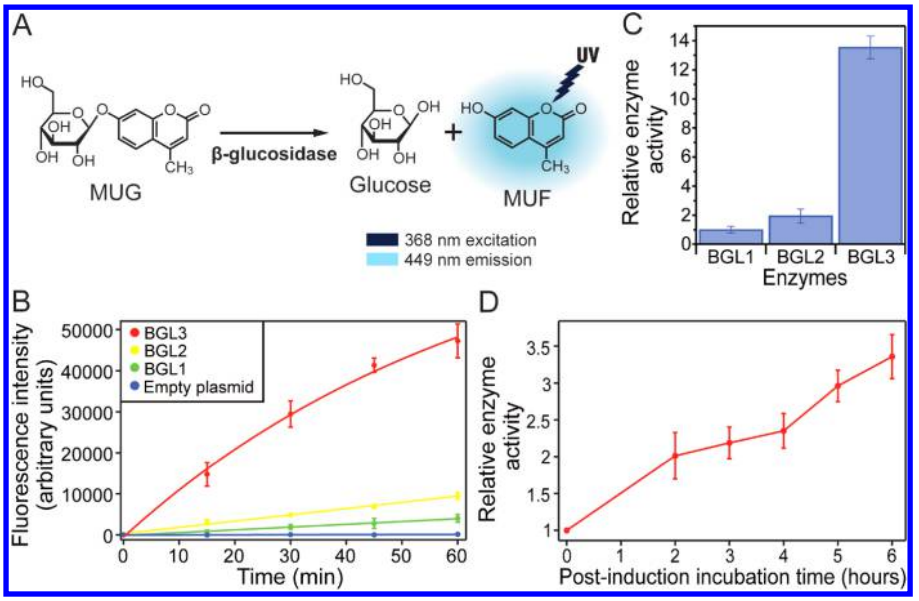

Figure 6. Expression optimization (single and multipoint) assay to discover highly active BGL. (A) Chemical scheme showing the enzymatic hydrolysis of 4-methylumbelliferyl β-D-glucopyranoside (MUG) to 4-methylumbelliferone (MUF) by a β-glucosidase (BGL). (B) Activity of three different BGLs in the presence of 2 mM MUG measured by fluorescence intensity (λ_{ex} = 369 nm and λ_{em} = 449 nm) over 60 min. (C) Comparison of the rates of activity for the three enzymes relative to the lowest (BGL1). (D) Induction profile of BGL3 over 6 h on the AIMS. For (B–D), error bars represent ±1 standard deviation across triplicates.

stop solution) and 32 actuation electrodes to moving and mixing reagents with the induced culture, and five assay regions to measuring enzyme activity on device. After 4 h of induction at 37 °C, the cells were lysed and mixed with droplets containing the fluorogenic substrate MUG. Here, fluorescence over time was used as a read-out for enzyme activity. For future work, we propose that many other possible probes or proteins relying on fluorescence are compatible with the AIMS.

Fluorescence intensity for the enzymatic assay was measured directly on the device using a benchtop scanning well-plate reader and the enzyme activity curves are shown in Figure 6B. As expected, there is an increase in the fluorescence measured over time for the three different BGL enzymes while little or no activity is observed in our negative control (*i.e.*, an "empty" plasmid that does not contain any BGL). Specifically, in the single-point induction assay, the rate of activity measured by fluorescence was nearly identical for BGL1 and BGL2, but was significantly higher for BGL3. In fact, this rate is at least six times higher for BGL3 compared to the other two BGLs (Figure 6C). To further optimize the activity of BGL3, a multipoint induction assay was performed to determine the optimal postinduction incubation period for BGL3 expression (*i.e.*, prelysis). As shown in Figure 6D., the BGL3 showed highest expression (at least three times higher) after 6 h of induction and incubation compared to immediate induction and lysis (0 h). This is expected as the effect of postinduction incubation period affects the overall folding, accumulation and productivity of recombinant proteins in *E. coli* and therefore longer incubation times (>1 h) are more favorable.[72] As for the high activity of BGL3 (compared to the other tested BGLs) it is not well understood, however, some groups have hypothesized that higher salt concentrations (and at neutral pH 7.0) will induce higher activity of enzymes and faster growth for thermotolerant organisms like *Rhodothermus marinus*.[38,73] Furthermore, these organisms typically live in harsh environments and are required to constantly maintain their high-level thermostability and enzyme activity. Therefore, it is not a surprise that these enzymes can maintain their function and activity in a standard environment (*i.e.*, at room temperature, constant pH, *etc.*). Regardless, these results confirm that the AIMS is capable of automating induction and discovering enzymes that are possible candidates for biomass hydrolysis. We propose that the system described here may be useful in testing a variety of enzymes to identify more candidates for biofuel production and synthetic biology applications.

Future Work. We present the first automated induction microfluidics platform to monitor gene expression for synthetic biology applications using digital microfluidics. The AIMS enables (1) on-device OD reading, (2) in-line bacterial culture and induction in droplet format, and (3) analysis of enzyme expression and activity. We characterized our system by optimizing the OD measurement and the growth conditions for bacterial cell culture. The AIMS has a limit of detection of 0.035 OD units and was able to monitor bacterial growth at the microscale with no manual intervention over 5 h. Additionally, we tested the induction of a RFP gene in a pET expression vector using different IPTG concentrations to generate a dose–response curve and compared it to the macroscale experiment and found differences in their ultrasensitivity. Finally, we used the AIMS to measure the activity of three BGL enzymes directly on device after automated induction and optimized the highest active enzyme with different postinduction incubation conditions to optimize end-point activity.

Indeed, the work presented is proof-of-principle and is to enable users to adopt microfluidics (see github.com/shihmicrolab/AIMS) as a platform for their synthetic biology applications. As a first step to improve this system is to increase throughput expanding the repertoire of conditions to be tested. Current digital microfluidic devices (such as the one presented here) are usually designed with linear tracks of electrodes with coplanar connectivity which reduces the density of electrodes that can be placed on one device. There are methods in literature that improve the throughput of digital microfluidics, for example, hybrid microfluidics[35,36,39] which integrates digital

DOI: 10.1021/acssynbio.8b00025
ACS Synth. Biol. 2018, 7, 933–944

with droplet-in-flow microfluidics and has the potential of generating 100s of droplets while having the control and addressability of the droplets or printed circuit boards[74,75] since they enable vertical interconnects allowing more electrodes to be placed on one device. However, each of these systems has its advantages and disadvantages and the usage of these devices will depend on the applications. In addition, future developments in the automation system such as integration of in-line fluorescence and absorbance detection will make this technology an even more attractive solution for synthetic biology applications.

As described we have used the AIMS to automate bacterial cell culture and induction and optimizing conditions to enhance protein activity. Other possibilities on using this system (or a derivative thereof) may be useful for other applications in synthetic biology. For example, one can design a device for strain optimization to characterize the assortment of expression constructs or to test a diverse library of expression parts for their engineered strain.[8−11,76] Similarly, given the need to automate the synthetic biology workflow of design−build−test−learn, we propose that this microfluidic method is a first step for improving gene-to-protein expression from plasmid constructs that can be combined with other systems (*e.g.*, DNA assembly and transformation[35,36,77]) or *in silico* computer design programs[78−80] to potentially integrate with the AIMS to fully automate the synthetic biology workflow. With the possibility of these future additions, there is great potential for the application of microfluidics to automate induction, to analyze enzyme activity, and to be used for strain optimization.

■ ASSOCIATED CONTENT

Supporting Information

The Supporting Information is available free of charge on the ACS Publications website at DOI: 10.1021/acssynbio.8b00025.

Description of the fabrication procedure of the 3D enclosure with a figure showing the multiple layers of the AIMS; a table showing the strains and plasmids and primer sequences used in this study; schematic of the plasmids; an image of a gel showing the PCR products; bill of materials list of the electronic components for the automation system (PDF)

Video S1, shows the automated induction process on our digital microfluidic devices (MPG)

Genbank files of the plasmids (ZIP)

■ AUTHOR INFORMATION

Corresponding Author

*Tel: (514) 848-2424 x7579. E-mail: steve.shih@concordia.ca.

ORCID

Steve C. C. Shih: 0000-0003-3540-0808

Present Address

‖1455 de Maisonneuve Blvd., EV16.189, Montreal, Quebec H3G 1M8, Canada.

Author Contributions

M.C.H. and S.C.C.S designed the experiments. M.C.H. and P.Q.N.V. fabricated the DMF devices with the help of H.S and F.A. M.C.H. and P.Q.N.V. designed the AIMS and P.Q.N.V. wrote the software to operate the experiments. M.C.H. and P.Q.N.V. carried out the experiments on- and off-chip and analyzed the data with S.C. C.S., M.C.H., and S.C.C.S. wrote the paper and prepared the figures, and all authors reviewed the final version of the manuscript before submission.

Notes

The authors declare no competing financial interest.

See github.com/shihmicrolab/AIMS for hardware and software information; breakdown of the savings in costs, manual intervention, and hands-on time for the macroscale and AIMS.

■ ACKNOWLEDGMENTS

We thank Vincent Martin's laboratory for donating plasmids and strains and for his advice on this manuscript. We also thank David Kwan and Aashiq Kachroo for their advice on the manuscript. We thank the Natural Sciences and Engineering Research Council (NSERC), the Fonds de Recherche Nature et technologies (FRQNT), and the Canadian Foundation of Innovation (CFI) for funding. M.C.H. thanks Concordia University for an undergraduate scholarship (USRA), P.Q.N.V thanks NSERC, and H.S and F.A. thanks Concordia University for FRS funding.

■ REFERENCES

(1) Lienert, F., Lohmueller, J. J., Garg, A., and Silver, P. A. (2014) Synthetic biology in mammalian cells: next generation research tools and therapeutics. *Nat. Rev. Mol. Cell Biol. 15*, 95−107.

(2) Slomovic, S., Pardee, K., and Collins, J. J. (2015) Synthetic biology devices for in vitro and in vivo diagnostics. *Proc. Natl. Acad. Sci. U. S. A. 112*, 14429−14435.

(3) DeLoache, W. C., Russ, Z. N., Narcross, L., Gonzales, A. M., Martin, V. J., and Dueber, J. E. (2015) An enzyme-coupled biosensor enables (S)-reticuline production in yeast from glucose. *Nat. Chem. Biol. 11*, 465−471.

(4) Zhang, F., Carothers, J. M., and Keasling, J. D. (2012) Design of a dynamic sensor-regulator system for production of chemicals and fuels derived from fatty acids. *Nat. Biotechnol. 30*, 354−359.

(5) Beller, H. R., Lee, T. S., and Katz, L. (2015) Natural products as biofuels and bio-based chemicals: fatty acids and isoprenoids. *Nat. Prod. Rep. 32*, 1508−1526.

(6) Klein-Marcuschamer, D., Santos, C. N., Yu, H., and Stephanopoulos, G. (2009) Mutagenesis of the bacterial RNA polymerase alpha subunit for improvement of complex phenotypes. *Appl. Environ. Microbiol. 75*, 2705−2711.

(7) Wang, H. H., Isaacs, F. J., Carr, P. A., Sun, Z. Z., Xu, G., Forest, C. R., and Church, G. M. (2009) Programming cells by multiplex genome engineering and accelerated evolution. *Nature 460*, 894−898.

(8) Anderson, J. C., Dueber, J. E., Leguia, M., Wu, G. C., Goler, J. A., Arkin, A. P., and Keasling, J. D. (2010) BglBricks: A flexible standard for biological part assembly. *J. Biol. Eng. 4*, 1.

(9) Davis, J. H., Rubin, A. J., and Sauer, R. T. (2011) Design, construction and characterization of a set of insulated bacterial promoters. *Nucleic Acids Res. 39*, 1131−1141.

(10) Mutalik, V. K., Guimaraes, J. C., Cambray, G., Lam, C., Christoffersen, M. J., Mai, Q. A., Tran, A. B., Paull, M., Keasling, J. D., Arkin, A. P., and Endy, D. (2013) Precise and reliable gene expression via standard transcription and translation initiation elements. *Nat. Methods 10*, 354−360.

(11) Balzer, S., Kucharova, V., Megerle, J., Lale, R., Brautaset, T., and Valla, S. (2013) A comparative analysis of the properties of regulated promoter systems commonly used for recombinant gene expression in Escherichia coli. *Microb. Cell Fact. 12*, 26.

(12) Baneyx, F. (1999) Recombinant protein expression in Escherichia coli. *Curr. Opin. Biotechnol. 10*, 411−421.

(13) Jonasson, P., Liljeqvist, S., Nygren, P. A., and Stahl, S. (2002) Genetic design for facilitated production and recovery of recombinant proteins in Escherichia coli. *Biotechnol. Appl. Biochem. 35*, 91−105.

(14) Guzman, L. M., Belin, D., Carson, M. J., and Beckwith, J. (1995) Tight regulation, modulation, and high-level expression by vectors

containing the arabinose PBAD promoter. *J. Bacteriol. 177*, 4121−4130.
(15) Sorensen, H. P., and Mortensen, K. K. (2005) Advanced genetic strategies for recombinant protein expression in Escherichia coli. *J. Biotechnol. 115*, 113−128.
(16) Studier, F. W., Rosenberg, A. H., Dunn, J. J., and Dubendorff, J. W. (1990) Use of T7 RNA polymerase to direct expression of cloned genes. *Methods Enzymol. 185*, 60−89.
(17) Tegel, H., Ottosson, J., and Hober, S. (2011) Enhancing the protein production levels in Escherichia coli with a strong promoter. *FEBS J. 278*, 729−739.
(18) Jensen, P. R., Westerhoff, H. V., and Michelsen, O. (1993) The use of lac-type promoters in control analysis. *Eur. J. Biochem. 211*, 181−191.
(19) Grabski, A., Mehler, M., and Drott, D. (2003) Unattended high-density cell growth and induction of protein expression with the Overnight Express Autoinduction System. *InNovations 17*, 3−8.
(20) Studier, F. W. (2005) Protein production by auto-induction in high-density shaking cultures. *Protein Expression Purif. 41*, 207−234.
(21) Tsao, C. Y., Hooshangi, S., Wu, H. C., Valdes, J. J., and Bentley, W. E. (2010) Autonomous induction of recombinant proteins by minimally rewiring native quorum sensing regulon of E. coli. *Metab. Eng. 12*, 291−297.
(22) Nocadello, S., and Swennen, E. F. (2012) The new pLAI (lux regulon based auto-inducible) expression system for recombinant protein production in Escherichia coli. *Microb. Cell Fact. 11*, 3.
(23) Briand, L., Marcion, G., Kriznik, A., Heydel, J. M., Artur, Y., Garrido, C., Seigneuric, R., and Neiers, F. (2016) A self-inducible heterologous protein expression system in Escherichia coli. *Sci. Rep. 6*, 33037.
(24) Grabski, A., Mehler, M., and Drott, D. (2005) The Overnight Express Autoinduction System: High-density cell growth and protein expression while you sleep. *Nat. Methods 2*, 233−235.
(25) Faust, G., Stand, A., and Weuster-Botz, D. (2015) IPTG can replace lactose in auto-induction media to enhance protein expression in batch-cultured Escherichia coli. *Eng. Life Sci. 15*, 824−829.
(26) Huang, H., and Densmore, D. (2014) Integration of microfluidics into the synthetic biology design flow. *Lab Chip 14*, 3459−3474.
(27) Linshiz, G., Jensen, E., Stawski, N., Bi, C., Elsbree, N., Jiao, H., Kim, J., Mathies, R., Keasling, J. D., and Hillson, N. J. (2016) End-to-end automated microfluidic platform for synthetic biology: from design to functional analysis. *J. Biol. Eng. 10*, 3.
(28) Luke, C. S., Selimkhanov, J., Baumgart, L., Cohen, S. E., Golden, S. S., Cookson, N. A., and Hasty, J. (2016) A microfluidic platform for long-Term monitoring of algae in a dynamic environment. *ACS Synth. Biol. 5*, 8−14.
(29) Nayak, S., Sridhara, A., Melo, R., Richer, L., Chee, N. H., Kim, J., Linder, V., Steinmiller, D., Sia, S. K., and Gomes-Solecki, M. (2016) Microfluidics-based point-of-care test for serodiagnosis of Lyme Disease. *Sci. Rep. 6*, 35069.
(30) Kong, D. S., Thorsen, T. A., Babb, J., Wick, S. T., Gam, J. J., Weiss, R., and Carr, P. A. (2017) Open-source, community-driven microfluidics with Metafluidics. *Nat. Biotechnol. 35*, 523−529.
(31) Jebrail, M. J., Bartsch, M. S., and Patel, K. D. (2012) Digital microfluidics: a versatile tool for applications in chemistry, biology and medicine. *Lab Chip 12*, 2452−2463.
(32) Samiei, E., Tabrizian, M., and Hoorfar, M. (2016) A review of digital microfluidics as portable platforms for lab-on a-chip applications. *Lab Chip 16*, 2376−2396.
(33) Choi, K., Ng, A. H., Fobel, R., and Wheeler, A. R. (2012) Digital microfluidics. *Annu. Rev. Anal. Chem. 5*, 413−440.
(34) Ben Yehezkel, T., Rival, A., Raz, O., Cohen, R., Marx, Z., Camara, M., Dubern, J. F., Koch, B., Heeb, S., Krasnogor, N., Delattre, C., and Shapiro, E. (2016) Synthesis and cell-free cloning of DNA libraries using programmable microfluidics. *Nucleic Acids Res. 44*, e35.
(35) Gach, P. C., Shih, S. C. C., Sustarich, J., Keasling, J. D., Hillson, N. J., Adams, P. D., and Singh, A. K. (2016) A Droplet Microfluidic Platform for Automating Genetic Engineering. *ACS Synth. Biol. 5*, 426−433.
(36) Shih, S. C. C., Goyal, G., Kim, P. W., Koutsoubelis, N., Keasling, J. D., Adams, P. D., Hillson, N. J., and Singh, A. K. (2015) A versatile microfluidic device for automating synthetic biology. *ACS Synth. Biol. 10*, 1151−1164.
(37) Choi, Y. J., Morel, L., Le Francois, T., Bourque, D., Bourget, L., Groleau, D., Massie, B., and Miguez, C. B. (2010) Novel, versatile, and tightly regulated expression system for Escherichia coli strains. *Appl. Environ. Microbiol. 76*, 5058−5066.
(38) Gladden, J. M., Park, J. I., Bergmann, J., Reyes-Ortiz, V., D'Haeseleer, P., Quirino, B. F., Sale, K. L., Simmons, B. A., and Singer, S. W. (2014) Discovery and characterization of ionic liquid-tolerant thermophilic cellulases from a switchgrass-adapted microbial community. *Biotechnol. Biofuels 7*, 15.
(39) Shih, S. C. C., Gach, P. C., Sustarich, J., Simmons, B. A., Adams, P. D., Singh, S., and Singh, A. K. (2015) A droplet-to-digital (D2D) microfluidic device for single cell assays. *Lab Chip 15*, 225−236.
(40) Vo, P. Q. N., Husser, M., Ahmadi, F., Sinha, H., and Shih, S. C. C. (2017) Image-based feedback and analysis system for digital microfluidics. *Lab Chip 17*, 3437−3446.
(41) Au, S. H., Kumar, P., and Wheeler, A. R. (2011) A new angle on pluronic additives: advancing droplets and understanding in digital microfluidics. *Langmuir 27*, 8586−8594.
(42) Shih, S. C. C., Barbulovic-Nad, I., Yang, X., Fobel, R., and Wheeler, A. R. (2013) Digital microfluidics with impedance sensing for integrated cell culture and analysis. *Biosens. Bioelectron. 42*, 314−320.
(43) Shih, S. C. C., Mufti, N. S., Chamberlain, M. D., Kim, J., and Wheeler, A. R. (2014) A droplet-based screen for wavelength-dependent lipid production in algae. *Energy Environ. Sci. 7*, 2366−2375.
(44) Haynes, K. A., Ceroni, F., Flicker, D., Younger, A., and Silver, P. A. (2012) A sensitive switch for visualizing natural gene silencing in single cells. *ACS Synth. Biol. 1*, 99−106.
(45) Oishi, K., and Klavins, E. (2014) Framework for engineering finite state machines in gene regulatory networks. *ACS Synth. Biol. 3*, 652−665.
(46) Markley, A. L., Begemann, M. B., Clarke, R. E., Gordon, G. C., and Pfleger, B. F. (2015) Synthetic biology toolbox for controlling gene expression in the cyanobacterium Synechococcus sp. strain PCC 7002. *ACS Synth. Biol. 4*, 595−603.
(47) Redden, H., Morse, N., and Alper, H. S. (2015) The synthetic biology toolbox for tuning gene expression in yeast. *FEMS Yeast Res. 15*, 1−10.
(48) Takahashi, C. N., Miller, A. W., Ekness, F., Dunham, M. J., and Klavins, E. (2015) A low cost, customizable turbidostat for use in synthetic circuit characterization. *ACS Synth. Biol. 4*, 32−38.
(49) Al Taweel, A. M., Shah, Q., and Aufderheide, B. (2012) Effect of Mixing on Microorganism Growth in Loop Bioreactors. *Int. J. Chem. Eng. 2012*, 12.
(50) Paik, P., Pamula, V. K., and Fair, R. B. (2003) Rapid droplet mixers for digital microfluidic systems. *Lab Chip 3*, 253−259.
(51) Au, S. H., Shih, S. C. C., and Wheeler, A. R. (2011) Integrated microbioreactor for culture and analysis of bacteria, algae and yeast. *Biomed. Microdevices 13*, 41−50.
(52) Lu, H. W., Bottausci, F., Fowler, J. D., Bertozzi, A. L., Meinhart, C., and Kim, C. J. (2008) A study of EWOD-driven droplets by PIV investigation. *Lab Chip 8*, 456−461.
(53) Lee, C. P., Chen, H. C., and Lai, M. F. (2012) Electrowetting on dielectric driven droplet resonance and mixing enhancement in parallel-plate configuration. *Biomicrofluidics 6*, 12814−128148.
(54) Abdelgawad, M., Park, P., and Wheeler, A. R. (2009) Optimization of device geometry in single-plate digital microfluidics. *J. Appl. Phys. 105*, 094506.
(55) Zeng, J., and Korsmeyer, T. (2004) Principles of droplet electrohydrodynamics for lab-on-a-chip. *Lab Chip 4*, 265−277.

DOI: 10.1021/acssynbio.8b00025
ACS Synth. Biol. 2018, 7, 933−944

(56) Choi, K., Mudrik, J. M., and Wheeler, A. R. (2015) A guiding light: spectroscopy on digital microfluidic devices using in-plane optical fibre waveguides. *Anal. Bioanal. Chem. 407*, 7467−7475.
(57) Ceyssens, F., Witters, D., Grimbergen, T. V., Knez, K., Lammertyn, J., and Puers, R. (2013) Integrating optical waveguides in electrowetting-on-dielectric digital microfluidic chips. *Sens. Actuators, B 181*, 166−171.
(58) Chen, T., Dong, C., Gao, J., Jia, Y., Mak, P. I., Vai, M. I., and Martins, R. P. (2014) Natural discharge after pulse and cooperative electrodes to enhance droplet velocity in digital microfluidics. *AIP Adv. 4*, 047129.
(59) Chen, C. H., Tsai, S. L., Chen, M. K., and Jang, L. S. (2011) Effects of gap height, applied frequency, and fluid conductivity on minimum actuation voltage of electrowetting-on-dielectric and liquid dielectrophoresis. *Sens. Actuators, B 159*, 321−327.
(60) University of Cambridge (2009) International Genetically Engineered Machine (iGEM).
(61) Dueber, J. E., Mirsky, E. A., and Lim, W. A. (2007) Engineering synthetic signaling proteins with ultrasensitive input/output control. *Nat. Biotechnol. 25*, 660−662.
(62) Hooshangi, S., Thiberge, S., and Weiss, R. (2005) Ultrasensitivity and noise propagation in a synthetic transcriptional cascade. *Proc. Natl. Acad. Sci. U. S. A. 102*, 3581−3586.
(63) Barbulovic-Nad, I., Au, S. H., and Wheeler, A. R. (2010) A microfluidic platform for complete mammalian cell culture. *Lab Chip 10*, 1536−1542.
(64) Sista, R., Hua, Z., Thwar, P., Sudarsan, A., Srinivasan, V., Eckhardt, A., Pollack, M., and Pamula, V. (2008) Development of a digital microfluidic platform for point of care testing. *Lab Chip 8*, 2091−2104.
(65) Song, Y., Nikoloff, J. M., Fu, G., Chen, J., Li, Q., Xie, N., Zheng, P., Sun, J., and Zhang, D. (2016) Promoter Screening from Bacillus subtilis in Various Conditions Hunting for Synthetic Biology and Industrial Applications. *PLoS One 11*, e0158447.
(66) Stanton, B. C., Nielsen, A. A., Tamsir, A., Clancy, K., Peterson, T., and Voigt, C. A. (2014) Genomic mining of prokaryotic repressors for orthogonal logic gates. *Nat. Chem. Biol. 10*, 99−105.
(67) Ang, J., Harris, E., Hussey, B. J., Kil, R., and McMillen, D. R. (2013) Tuning response curves for synthetic biology. *ACS Synth. Biol. 2*, 547−567.
(68) Heinemann, J., Deng, K., Shih, S. C., Gao, J., Adams, P. D., Singh, A. K., and Northen, T. R. (2017) On-chip integration of droplet microfluidics and nanostructure-initiator mass spectrometry for enzyme screening. *Lab Chip 17*, 323−331.
(69) Steen, E. J., Kang, Y., Bokinsky, G., Hu, Z., Schirmer, A., McClure, A., Del Cardayre, S. B., and Keasling, J. D. (2010) Microbial production of fatty-acid-derived fuels and chemicals from plant biomass. *Nature 463*, 559−562.
(70) Peralta-Yahya, P. P., and Keasling, J. D. (2010) Advanced biofuel production in microbes. *Biotechnol. J. 5*, 147−162.
(71) Nakayama, S., Kiyoshi, K., Kadokura, T., and Nakazato, A. (2011) Butanol production from crystalline cellulose by cocultured Clostridium thermocellum and Clostridium saccharoperbutylacetonicum N1−4. *Appl. Environ. Microbiol. 77*, 6470−6475.
(72) Shin, C. S., Hong, M. S., Bae, C. S., and Lee, J. (1997) Enhanced production of human mini-proinsulin in fed-batch cultures at high cell density of Escherichia coli BL21(DE3)[pET-3aT2M2]. *Biotechnol. Prog. 13*, 249−257.
(73) Bjornsdottir, S. H., Blondal, T., Hreggvidsson, G. O., Eggertsson, G., Petursdottir, S., Hjorleifsdottir, S., Thorbjarnardottir, S. H., and Kristjansson, J. K. (2006) Rhodothermus marinus: physiology and molecular biology. *Extremophiles 10*, 1−16.
(74) Gong, J., and Kim, C. J. (2008) All-electronic droplet generation on-chip with real-time feedback control for EWOD digital microfluidics. *Lab Chip 8*, 898−906.
(75) Jebrail, M. J., Renzi, R. F., Sinha, A., Van De Vreugde, J., Gondhalekar, C., Ambriz, C., Meagher, R. J., and Branda, S. S. (2015) A solvent replenishment solution for managing evaporation of biochemical reactions in air-matrix digital microfluidics devices. *Lab Chip 15*, 151−158.
(76) Reider Apel, A., d'Espaux, L., Wehrs, M., Sachs, D., Li, R. A., Tong, G. J., Garber, M., Nnadi, O., Zhuang, W., Hillson, N. J., Keasling, J. D., and Mukhopadhyay, A. (2017) A Cas9-based toolkit to program gene expression in Saccharomyces cerevisiae. *Nucleic Acids Res. 45*, 496−508.
(77) Kong, D. S., Thorsen, T. A., Babb, J., Wick, S. T., Gam, J. J., Weiss, R., and Carr, P. A. (2017) Open-source, community-driven microfluidics with Metafluidics. *Nat. Biotechnol. 35*, 523−529.
(78) Salis, H. M. (2011) The ribosome binding site calculator. *Methods Enzymol. 498*, 19−42.
(79) Zhang, M., McLaughlin, J. A., Wipat, A., and Myers, C. J. (2017) SBOLDesigner 2: An Intuitive Tool for Structural Genetic Design. *ACS Synth. Biol. 6*, 1150−1160.
(80) Myers, C. J., Beal, J., Gorochowski, T. E., Kuwahara, H., Madsen, C., McLaughlin, J. A., Misirli, G., Nguyen, T., Oberortner, E., Samineni, M., Wipat, A., Zhang, M., and Zundel, Z. (2017) A standard-enabled workflow for synthetic biology. *Biochem. Soc. Trans. 45*, 793−803.

DOI: 10.1021/acssynbio.8b00025
ACS Synth. Biol. 2018, 7, 933−944